Shifted Circular Tokamak Equilibrium with Application Examples

Hua-sheng Xie (谢华生, huashengxie@gmail.com)
Institute for Fusion Theory and Simulation, Department of Physics,
Zhejiang University, Hangzhou, 310027, People's Republic of China

v1: March 16, 2013; Update: April 5, 2014

Abstract

We give a detailed description of large aspect ratio approximation ($\epsilon \equiv a/R_0 \ll 1$) Shafranov equilibrium, which is also called shifted circular equilibrium and related to s-α local equilibrium. Topics included: Jacobian and many other variables in both Shafranov coordinate and flux coordinate; comparing with direct numerical solutions; applications to GTC, orbit.m (trajectory following code), awcon.m (Alfvén wave continuum spectral code) and AMC (Alfvén eigen Mode Code). [draft]

1 Introduction

1.1 Flux surface shape

Defining the shifted circular equilibrium flux surface in terms of the usual cylindrical (R, ϕ, Z) coordinate

$$R = R_0 + r_s \cos\theta_s - \Delta(r_s), \tag{1a}$$
$$\phi_c = -\phi = -\zeta_s, \tag{1b}$$
$$Z = r_s \sin\theta_s, \tag{1c}$$

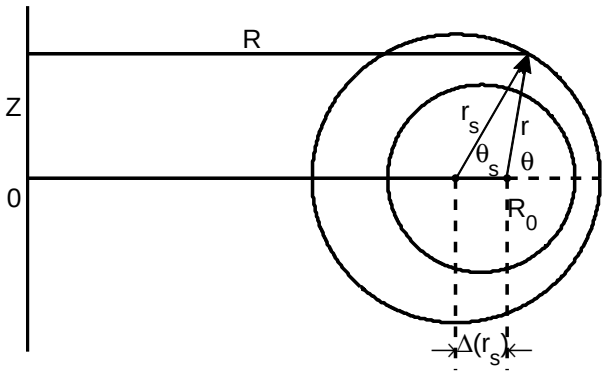

Figure 1: Flux surfaces for shifted circular equilibrium.

where R_0 is the major radius and the shift $\Delta(0) = 0$. The minus sign in (1b) is to keep Shafranov coordinate (r_s, θ_s, ζ_s) right handed, ϕ_c is for cylinder and ϕ for torus.

Fig.1 shows the flux surfaces and coordinate system. Note the difference between (r_s, θ_s, ζ_s) and usual torus coordinate (r, θ, ζ).

Hereafter, we normalize R_0 and on axis B_0 to unity. All the discussions are for axisymmetric equilibria.

1.2 Metric tensor and Jacobian

Euclidean coordinate $\mathbf{r}(x, y, z)$ in terms to arbitrary coordinate (u^1, u^2, u^3) with

$$x = x(u^1, u^2, u^3), \quad y = y(u^1, u^2, u^3), \quad z = z(u^1, u^2, u^3), \tag{2}$$

and visa versa

$$u^1 = u^1(x, y, z), \quad u^2 = u^2(x, y, z), \quad u^3 = u^3(x, y, z). \tag{3}$$

Covariant vector basis

$$\mathbf{e}_1 = \frac{\partial \mathbf{r}}{\partial u^1}, \quad \mathbf{e}_2 = \frac{\partial \mathbf{r}}{\partial u^2}, \quad \mathbf{e}_3 = \frac{\partial \mathbf{r}}{\partial u^3}, \tag{4}$$

contravariant basis

$$\mathbf{e}^1 = \nabla u^1, \quad \mathbf{e}^2 = \nabla u^2, \quad \mathbf{e}^3 = \nabla u^3, \tag{5}$$

with the relations

$$\mathbf{e}_i = \frac{\mathbf{e}^j \times \mathbf{e}^k}{\mathbf{e}^i \cdot (\mathbf{e}^j \times \mathbf{e}^k)}, \quad \mathbf{e}^i = \frac{\mathbf{e}_j \times \mathbf{e}_k}{\mathbf{e}_i \cdot (\mathbf{e}_j \times \mathbf{e}_k)}. \tag{6}$$

The covariant metric tensor

$$g_{ij} = g_{ji} := \begin{pmatrix} \mathbf{e}_1 \cdot \mathbf{e}_1 & \mathbf{e}_1 \cdot \mathbf{e}_2 & \mathbf{e}_1 \cdot \mathbf{e}_3 \\ \mathbf{e}_2 \cdot \mathbf{e}_1 & \mathbf{e}_2 \cdot \mathbf{e}_2 & \mathbf{e}_2 \cdot \mathbf{e}_3 \\ \mathbf{e}_3 \cdot \mathbf{e}_1 & \mathbf{e}_3 \cdot \mathbf{e}_2 & \mathbf{e}_3 \cdot \mathbf{e}_3 \end{pmatrix}, \tag{7}$$

the contraviant tensor

$$g^{ij} = g^{ji} := \begin{pmatrix} \mathbf{e}^1 \cdot \mathbf{e}^1 & \mathbf{e}^1 \cdot \mathbf{e}^2 & \mathbf{e}^1 \cdot \mathbf{e}^3 \\ \mathbf{e}^2 \cdot \mathbf{e}^1 & \mathbf{e}^2 \cdot \mathbf{e}^2 & \mathbf{e}^2 \cdot \mathbf{e}^3 \\ \mathbf{e}^3 \cdot \mathbf{e}^1 & \mathbf{e}^3 \cdot \mathbf{e}^2 & \mathbf{e}^3 \cdot \mathbf{e}^3 \end{pmatrix}, \tag{8}$$

and the Jacobian

$$\mathcal{J} = |\mathbf{e}_i \cdot (\mathbf{e}_j \times \mathbf{e}_k)| = \sqrt{|g_{ij}|}, \tag{9}$$

or inverse Jacobian

$$\mathcal{J}^{-1} = |\mathbf{e}^i \cdot (\mathbf{e}^j \times \mathbf{e}^k)| = \sqrt{|g^{ij}|}. \tag{10}$$

The transformation between covariant and contravariant basis are $\mathbf{e}_i = g_{ij}\mathbf{e}^j$ and $\mathbf{e}^i = g^{ij}\mathbf{e}_j$.

For axisymmetric coordinate (ψ, θ, ϕ) with $\nabla\phi = 1/R\hat{\phi}$, the transformation relations are (see also, Chap. 5 in Ref.[3])

$$\begin{pmatrix} \nabla\psi \\ \nabla\theta \\ \nabla\phi \end{pmatrix} = \begin{pmatrix} |\nabla\psi|^2 & \nabla\psi \cdot \nabla\theta & 0 \\ \nabla\theta \cdot \nabla\psi & |\nabla\theta|^2 & 0 \\ 0 & 0 & 1/R^2 \end{pmatrix} \begin{pmatrix} \nabla\theta \times \nabla\phi\mathcal{J} \\ \nabla\phi \times \nabla\psi\mathcal{J} \\ \nabla\psi \times \nabla\theta\mathcal{J} \end{pmatrix}, \tag{11}$$

and

$$\begin{pmatrix} \nabla\theta\times\nabla\phi\mathcal{J} \\ \nabla\phi\times\nabla\psi\mathcal{J} \\ \nabla\psi\times\nabla\theta\mathcal{J} \end{pmatrix} = \begin{pmatrix} |\nabla\theta|^2\mathcal{J}^2/R^2 & -\nabla\theta\cdot\nabla\psi\mathcal{J}^2/R^2 & 0 \\ -\nabla\psi\cdot\nabla\theta\mathcal{J}^2/R^2 & |\nabla\psi|^2\mathcal{J}^2/R^2 & 0 \\ 0 & 0 & R^2 \end{pmatrix} \begin{pmatrix} \nabla\psi \\ \nabla\theta \\ \nabla\phi \end{pmatrix}, \tag{12}$$

which also gives

$$|\nabla\psi|^2|\nabla\theta|^2 - (\nabla\theta\cdot\nabla\psi)^2 = \frac{R^2}{\mathcal{J}}. \tag{13}$$

1.3 Flux coordinates

For straight field line flux coordinates[6]: (1) Choose $\nu(\psi,\theta)$ for $\zeta = \phi - \nu$ such that $q \equiv \mathbf{B}\cdot\nabla\zeta/\mathbf{B}\cdot\nabla\theta = q(\psi)$[1], with $r = r(\psi)$ a radial-like flux coordinate; (2) Additional freedom of choosing θ to select Jacobian $\mathcal{J} = [\nabla\zeta\cdot(\nabla\psi\times\nabla\theta)]^{-1}$. Examples are: Hamada coordinates $\mathcal{J} = \mathcal{J}_H(\psi)$ and Boozer coordinates $\mathcal{J} = \hat{\mathcal{J}}_B(\psi)/B^2$.

Another form of Boozer coordinate is

$$\mathbf{B} = g(\psi)\nabla\zeta + I(\psi)\nabla\theta + \delta(\psi,\theta)\nabla\psi. \tag{14}$$

Noticing $\nabla\phi = \hat{\phi}/R$ and using $\mathbf{B}\cdot\nabla\zeta = \mathbf{B}\cdot\nabla\phi - \partial_\theta\nu\mathbf{B}\cdot\nabla\theta$, and $\mathbf{B}\cdot\nabla\phi = g/R^2$, and $\mathbf{B}\cdot\nabla\theta = 1/(\mathcal{J}q)$,

$$\frac{\partial\nu}{\partial\theta} = \frac{gq\mathcal{J}}{R^2} - q. \tag{15}$$

Note that the solution $\nu(\psi,\theta)$ can involve an arbitrary function of ψ and the Jacobian in (ψ,θ,ϕ) system is equal to that in (ψ,θ,ζ) system, $\mathcal{J}^{-1} = \nabla\zeta\cdot(\nabla\psi\times\nabla\theta) = \nabla\phi\cdot(\nabla\psi\times\nabla\theta)$.

The mixed representation of $\mathbf{B}$ (covariant for B_t, contravariant for B_p)

$$\mathbf{B} = g(\psi)\nabla\zeta + \nabla\zeta\times\nabla\psi_p, \tag{16}$$

is often more convenient than the general (contravariant) flux representaion

$$\mathbf{B} = \nabla\psi\times\nabla\theta + \nabla\zeta\times\nabla\psi_p, \tag{17}$$

or Clebsch representation

$$\mathbf{B} = \nabla\alpha(\psi,\theta,\zeta)\times\nabla\psi = \nabla(\zeta - q\theta)\times\nabla\psi, \tag{18}$$

where $\psi = \psi_t = \Psi_t/2\pi$ and $\psi_p = \Psi_p/2\pi$ are related to the toroidal and poloidal fluxes.

Using (12), we can convert (16) to covariant form

$$\mathbf{B} = g(\psi)\nabla\zeta + \Big(\psi_p'\frac{\mathcal{J}}{R^2}|\nabla\psi|^2\Big)\nabla\theta + \Big(-\psi_p'\frac{\mathcal{J}}{R^2}\nabla\psi\cdot\nabla\theta\Big)\nabla\psi, \tag{19}$$

where $\psi_p' = d\psi_p/d\psi = 1/q(\psi)$ and $\mathcal{J} = [\nabla\zeta\cdot(\nabla\psi_p\times\nabla\theta)]^{-1}$.

Using (14) and (17), in Boozer coordinate

$$B^2 = \mathbf{B}_i\cdot\mathbf{B}^i = g(\psi)\mathcal{J}^{-1} + \frac{I(\psi)}{q(\psi)}\mathcal{J}^{-1}, \tag{20}$$

[1]Note: For non-flux coordinates, an average definition is $q(\psi) \equiv \langle\mathbf{B}\cdot\nabla\zeta/\mathbf{B}\cdot\nabla\theta\rangle_\theta$.

i.e., $\mathcal{J}_B = [g(\psi) + I(\psi)/q(\psi)]/B^2$.

In general, we may deform new flux coordinates using (Chap. 6 in Ref.[4])

$$\theta_F = \theta_f + \frac{d\psi_p}{dr_f} G(r_f, \theta_f, \zeta_f), \quad \zeta_F = \zeta_f + \frac{d\psi_t}{dr_f} G(r_f, \theta_f, \zeta_f). \tag{21}$$

Here, we mainly interested in the below two types of flux coordinates

$$\theta_f = \theta + \frac{d\psi_p}{dr} G(r, \theta, \zeta), \quad \zeta_f = \zeta, \tag{22}$$

and

$$\theta_f = \theta, \quad \zeta_f = \zeta - \frac{d\psi_t}{dr} G(r, \theta, \zeta). \tag{23}$$

1.4 Grad-Shafranov equation

The Grad-Shafranov equation for ψ is [1]

$$\nabla \cdot \frac{\psi}{qR^2} + q\frac{dp}{d\psi} + \frac{gq}{R^2}\frac{dg}{d\psi} = 0, \tag{24}$$

with $d\psi/d\psi_p = q(\psi_p)$. Note, here $p = \beta/2$, with β the plasma beta.

We consider low β equilibrium with $\beta \sim \epsilon^2$. For boundary condition given by a circular conducting wall, to lowest order the equilibrium constant ψ surfaces are concentric circles. To second order, the flux surfaces are shifted circles[2], which are called Shafranov shift[5]. The third order will bring elliptical and triangular[3], which will be neglected in this document.

Some orderings: $\psi \sim \epsilon^2$, $g = 1 + g_2$ with $g_2 \sim O(\epsilon^2)$. Since $\mathbf{B} \cdot \hat{\phi} = 1 + g_2$, $\psi = \int \mathbf{B} \cdot \nabla\phi r dr = (r^2/2)[1 + O(\epsilon^2)]$, the term ϵ^2 contributes only to ellipticity and triangularity and can be ignored, then $\nabla\psi = r\nabla r$ and $df/d\psi = (1/r)df/dr$.

Here also means the solution of (24) is

$$\psi(R, Z) = \frac{r^2}{2} = \frac{(R - 1 + \Delta)^2 + Z^2}{2}. \tag{25}$$

2 Solving the Shafranov Equilibrium

Here, we solve (24) to order ϵ^2 to get the shift $\Delta(r)$.

2.1 Calculate the shift $\Delta(r)$

In this subsection, we calculate using **Shafranov coordinate** and omit the subscript indicates.

[2] So, any calculations of concentric circle equilibrium to order ϵ^2 without shift are meaningless. [However, you can argue this.][How about zero β case?]

[3] J. M. Greene, J. L. Johnson and K. E. Weimer, Tokamak Equilibrium, Physics of Fluids, 1971, 14, 671-683.

This part is mainly[4] follow White 2001 book[1], with corrections of typos.

Partial derivatives

$$\frac{\partial R}{\partial r} = \cos\theta - \Delta', \qquad \frac{\partial R}{\partial \theta} = -r\sin\theta, \tag{26}$$

$$\frac{\partial Z}{\partial r} = \sin\theta, \qquad \frac{\partial Z}{\partial \theta} = r\cos\theta, \tag{27}$$

where $\Delta' = d\Delta/dr \sim \epsilon$.

Using implicit function theorem

$$\frac{\partial u}{\partial x} = -\frac{\partial(F,G)}{\partial(x,v)} \Big/ \frac{\partial(F,G)}{\partial(u,v)}, \cdots \tag{28}$$

with

$$F(x,y;u,v) = 1 + r\cos\theta - \Delta - R, \qquad G(x,y;u,v) = r\sin\theta - Z, \tag{29}$$

and $u = r$, $v = \theta$, $x = R$ and $y = Z$, we get

$$\begin{pmatrix} \partial r/\partial R & \partial r/\partial Z \\ \partial\theta/\partial R & \partial\theta/\partial Z \end{pmatrix} = \frac{1}{r(1-\Delta'\cos\theta)} \begin{pmatrix} r\cos\theta & r\sin\theta \\ -\sin\theta & \cos\theta - \Delta' \end{pmatrix}. \tag{30}$$

Some necessary expressions for Grad-Shafranov euqaiton can be calculated

$$\nabla r = \frac{\cos\theta}{1-\Delta'\cos\theta}\hat{R} + \frac{\sin\theta}{1-\Delta'\cos\theta}\hat{Z}, \tag{31}$$

$$\nabla\theta = -\frac{\sin\theta}{r(1-\Delta'\cos\theta)}\hat{R} + \frac{(\cos\theta - \Delta')}{r(1-\Delta'\cos\theta)}\hat{Z}, \tag{32}$$

$$\mathcal{J} = [\nabla\phi\cdot(\nabla r\times\nabla\theta)]^{-1} = rR(1-\Delta'\cos\theta), \tag{33}$$

$$\frac{1}{\mathcal{J}}\frac{\partial}{\partial\theta}\Big(\frac{\mathcal{J}\nabla\theta\cdot\nabla\psi}{R^2 q}\Big) = -\frac{\Delta'\cos\theta}{q} + O(\epsilon^2), \tag{34}$$

$$\frac{1}{\mathcal{J}}\frac{\partial}{\partial r}\Big(\frac{\mathcal{J}\nabla r\cdot\nabla\psi}{R^2 q}\Big) = \frac{1}{rR(1-\Delta'\cos\theta)}\frac{\partial}{\partial r}\Big[\frac{r^2}{q}(1+\Delta'\cos\theta - r\cos\theta + O(\epsilon^2))\Big], \tag{35}$$

$$\nabla\cdot\Big(\frac{1}{R^2 q}\nabla\psi\Big) = (34)+(35) = -\frac{\Delta'\cos\theta}{q} + \frac{1}{r}\Big(\frac{r^2}{q}\Big)'(1+2\Delta'\cos\theta - 2r\cos\theta) + \frac{r}{q}(\Delta''\cos\theta - \cos\theta). \tag{36}$$

Substituting into (24) and keeping only the terms independent of θ, we get

$$p' + gg' + \frac{f}{r}(rf)' = 0, \tag{37}$$

which are all $O(\epsilon)$, with $f \equiv r/q$. For applications, we choose $p(r)$ and $q(r)$ freely to determine g. While, since $g_2 \sim O(\epsilon^2)$, we may use $g = 1$ for approximation.

Terms with $\cos\theta$ give

$$\Delta'' + \Big[\frac{2(rf)'}{rf} - \frac{1}{r}\Big]\Delta' - \frac{2(rf)'}{f} - 1 - \frac{2rgg'}{f^2} = 0. \tag{38}$$

[4]See also Ref.?? for the form with R_0 and B_0 written out explicitly.

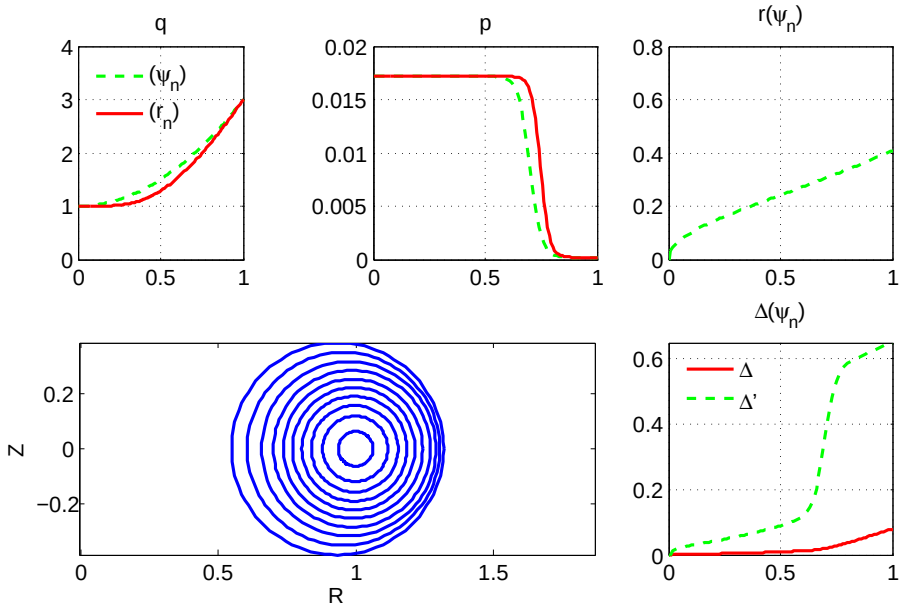

Figure 2: Calculate the Shafranov shift.

Eliminate gg' in (38) and note

$$(rf^2\Delta')' = \Big[\frac{(rf)^2\Delta'}{r}\Big]' = rf^2\Big\{\Delta'' + \big[\frac{2(rf)'}{rf} - \frac{1}{r}\big]\Delta'\Big\}, \tag{39}$$

we get

$$\Delta' = \frac{1}{rf^2}\int_0^r (f^2 - 2rp')rdr, \tag{40}$$

and

$$\Delta = \int_0^r \frac{dr}{rf^2}\int_0^r (f^2 - 2rp')rdr. \tag{41}$$

Note that normally $p' < 0$ so $\Delta' > 0$. One should also note that to avoid the intersecting of two flux surfaces, we need $\Delta' dr < dr$, i.e.,

$$\boldsymbol{\Delta' < 1}. \tag{42}$$

An estimation of Δ' with $q = 3$, $a = 0.1$, $p' \simeq -\epsilon \simeq -a$, gives $\Delta' \simeq \frac{q^2}{a^3}\left[\frac{1}{4}\frac{a^4}{q^2} + \frac{2}{3}a^3p'\right] \simeq \frac{a}{4} + \frac{2}{3}q^2p' \simeq q^2\epsilon \simeq 1$. We can see that Δ' is not that small as $O(\epsilon)$ but $O(q^2\epsilon)$! Usually, a more reasonable ordering of q is $O(\epsilon^{-1/2})$[5], which will bring many troubles. To avoid this, we'd better use even smaller β, e.g., $O(\epsilon^3)$.

A typical result is shown in Fig.2.

For ballooning mode, we must consider the Shafranov shift. While, note that $\Delta \neq 0$ even though $p' = 0$. So, for Alfvén wave (AW) or eigenmodes (AEs) and many other applications, one may also consider the shift[6].

[5] However, few analytical results can be found in literatures using this ordering.

[6] Many calculations or simulations showed that the shift effects are not that important for modes which are not driven by pressure gradient, e.g., zero-β ITG. So, choose as you like: simple or rigorous.

For reference, the contravariant metric elements is calculated

$$g^{ij} = \left\{\nabla u^i \cdot \nabla u^j\right\} \simeq \begin{pmatrix} 1+2\Delta'\cos\theta & -\Delta'\sin\theta/r & 0 \\ -\Delta'\sin\theta/r & 1/r^2 & 0 \\ 0 & 0 & 1-2r\cos\theta \end{pmatrix}, \tag{43}$$

and covariant

$$g_{ij} = \left\{\frac{\partial \mathbf{r}}{\partial u^i} \cdot \frac{\partial \mathbf{r}}{\partial u^j}\right\} \simeq \begin{pmatrix} 1-2\Delta'\cos\theta & r\Delta'\sin\theta & 0 \\ r\Delta'\sin\theta & r^2 & 0 \\ 0 & 0 & 1+2r\cos\theta \end{pmatrix}, \tag{44}$$

and $\mathcal{J} = \sqrt{|g^{ij}|^{-1}} \simeq r[1+(r-\Delta')\cos\theta]$, which is consistent with (33).

2.2 Comparing with numerical solver

To give an intuitive impression of errors of the shifted circular approximation, we comparing the results with direct numerical solver of G-S equation.

Numerical solution (VMOMS[7] code) of Grad-Shafranov equation shows that shift-circular flux surface geometry is adequate for low β. In Fig.3, $\epsilon = a/R = 0.25$.

For low $\beta \sim \epsilon^2$ ($\beta_1 = 0.0403$), the elongation $E(E \sim 1+10^{-2})$ and triangularity T ($\sim 10^{-4}$) effects are very small and can be omitted. However, when β is larger, this shifted circular equilibrium would not valid any more, as shown in the Fig.3 for $\beta = 0.2015$.

Fig.4 shows that Eq.(41) can calculate the Shafranov shift correctly.

2.3 Forms in Shafranov coordinate

Neglecting order ϵ^2, using (16), for toroidal field[2]

$$B_t(r,\theta) = \frac{g}{R} = B_{t0}(r)(1-r\cos\theta) \simeq 1-r\cos\theta, \tag{45}$$

where $B_{t0} = I/R_0 \simeq 1$. For the poloidal field

$$B_p = \frac{r}{q}|\nabla\phi \times \nabla r| = \frac{r}{qR(1-\Delta'\cos\theta)} \simeq \frac{r}{q}[1-(r-\Delta')\cos\theta], \tag{46}$$

One can find that q does not measure the local field line pitch

$$\frac{\mathbf{B}\cdot\nabla\phi}{\mathbf{B}\cdot\nabla\theta} = q[1-(r+\Delta')\cos\theta], \tag{47}$$

which varies on θ. Thus, the Shafranov coordinate is not a flux coordinate[7].

Giving a flux coordinate $\theta_f = \theta + K(r,\theta)$ and keeping $\zeta_f = \zeta$ and $r_f = r$, we have

$$\frac{\mathbf{B}\cdot\nabla\phi}{\mathbf{B}\cdot\nabla\theta_f} = \frac{\mathbf{B}\cdot\nabla\zeta}{\mathbf{B}\cdot\nabla\theta}\frac{1}{1+\partial_\theta K} = \frac{q}{1+\partial_\theta K}[1-(r+\Delta')\cos\theta] = q, \tag{48}$$

[7]This is also true for $\Delta(r) = 0$ concentric circle case!

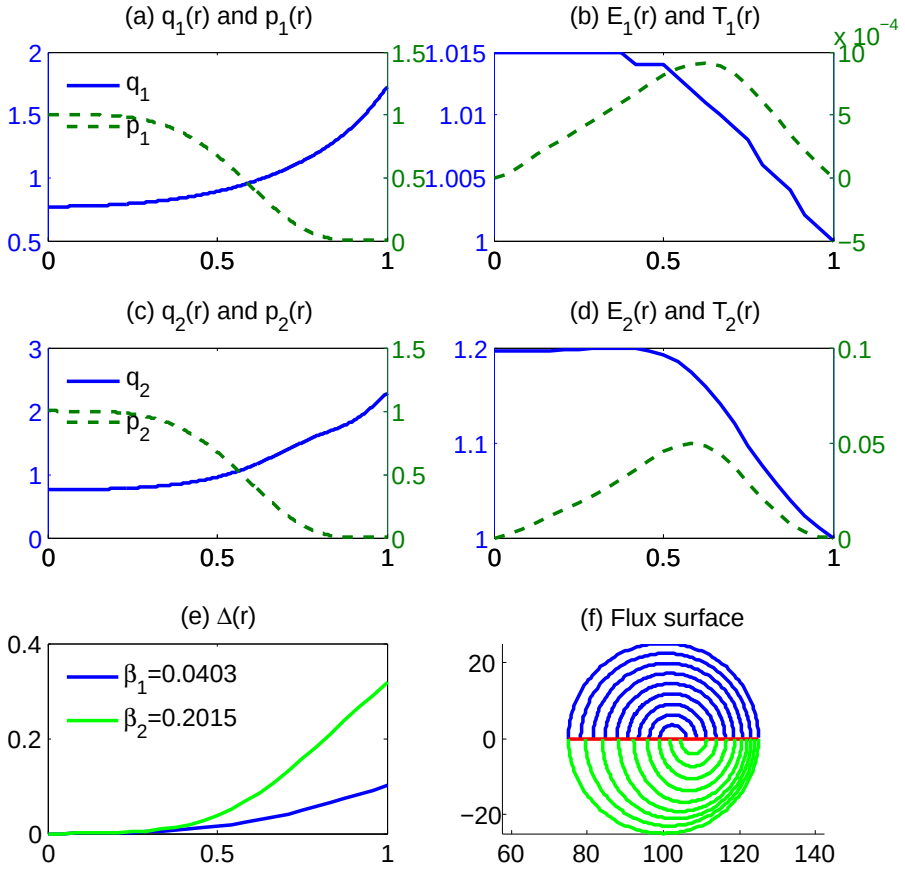

Figure 3: q and p (normalized on axis) profiles for (a) $\beta_1 = 0.0403$ and (c) $\beta_2 = 0.2015$. (b) and (d), the corresponding elongation E and triangularity T. (e), the corresponding Shafranov shift. (f), the flux surface contour.

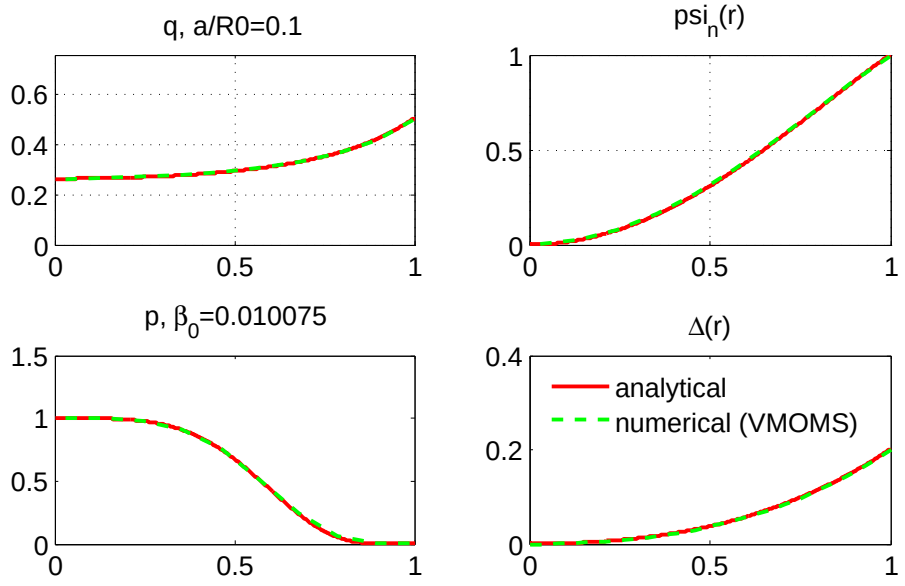

Figure 4: $\Delta(r)$, analytical vs. numerical (VMOMS).

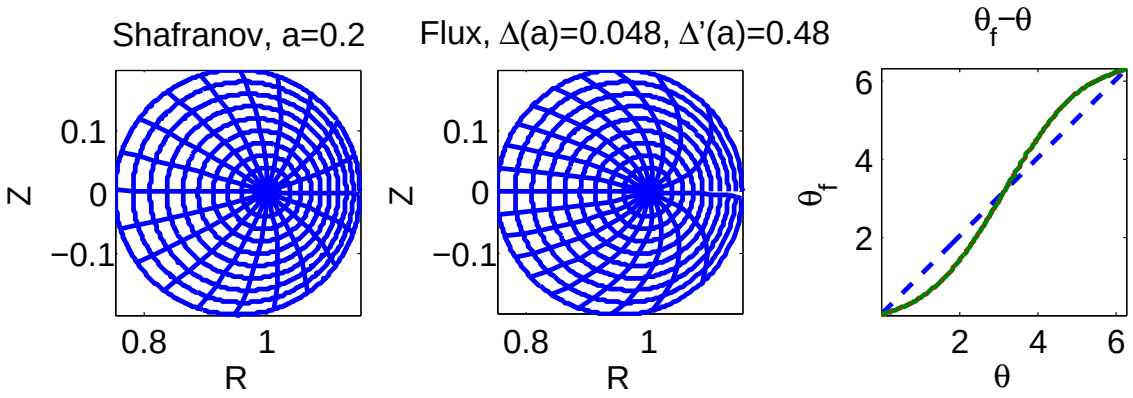

Figure 5: Shafranov coordinate and flux coordinate.

which gives

$$\partial_\theta K = -(r + \Delta') \cos\theta, \tag{49}$$

i.e.,

$$\theta_f = \theta - (r + \Delta') \sin\theta. \tag{50}$$

Fig. 5 shows the difference between Shafranov coordinate[8] and flux coordinate. To plot this figure, we need the relation $\theta(\theta_f)$, which is not explicit, instead of $\theta_f(\theta)$ in (50). We calculate it using 1D interpolation instead of solving inverse function, as below

```
theta0=1e-5:pi/N:2*pi;
thetaf=theta0-(r+dlp).*sin(theta0); % Boozer coordinate
thetaftmp=theta0;
% cal theta_s using interp, since the inverse function is not explicit
theta=interp1(thetaf,theta0,thetaftmp);
xf=1-dl+r.*cos(theta);
zf=r.*sin(theta);
```

However, since $(r + \Delta') \sim O(\epsilon)$, we can also use the approximation

$$\theta = \theta_f + (r + \Delta') \sin\theta_f + O(\epsilon^2). \tag{51}$$

Using (21)-(23), another choice of flux coordinate is keeping $\theta_f = \theta$ and $r_f = r$ but $\zeta_f = \zeta - \nu(r, \theta)$, with

$$\nu = -\Big(- K \frac{d_r \psi_p}{d_r \psi_t} \Big) = -q(r + \Delta') \sin\theta. \tag{52}$$

One can also obtain this result via (15).

2.4 Forms in Boozer coordinate

Note (31), (32) and $\nabla\psi_p = \nabla\psi/q = r\nabla r/q$, rewrite (16) to covariant representation similar as (14) using (19)

$$\mathbf{B} = g(\psi)\nabla\phi + \frac{r^2}{qR(1 - \Delta'\cos\theta)}\nabla\theta + \frac{\Delta'\sin\theta}{qR(1 - \Delta'\cos\theta)}\nabla\psi. \tag{53}$$

[8]Here is also an equal arc coordinate.

Noting $q(r) = \frac{\boldsymbol{B}\cdot\boldsymbol{\nabla}\phi}{\boldsymbol{B}\cdot\boldsymbol{\nabla}\theta_b}$, and using[9]

$$\frac{\partial\theta_b}{\partial\theta} = \frac{1}{R(1-\Delta'\cos\theta)}(R^2|r\nabla\theta_b|^2) \simeq \frac{1}{R(1+\Delta'\cos\theta)} \tag{54}$$

i.e.,

$$\theta_b = \theta - (r+\Delta')\sin\theta, \tag{55}$$

where $|r\nabla\theta_b|^2 = 1 - 2(r+\Delta')\cos\theta$, we can tranform (53) to Boozer form [need check $\delta(\psi,\theta)$]

$$\mathbf{B} = \underbrace{g(\psi)\nabla\phi}_{O(1)} + \underbrace{\frac{r^2}{q}\nabla\theta_b}_{O(\epsilon)} + \underbrace{\frac{\Delta'\sin\theta}{q}\nabla\psi}_{O(\epsilon^2)}, \tag{56}$$

which gives $I = r^2/q$. Since the $\delta(\psi,\theta_b)$ term is $O(\epsilon^2)$ and complicated, for applications, we may set it to zero, i.e., use $\delta = 0$ approximation. For g, we can use $g = 1$ approximation or calculate from (37)

$$g = 1 + g_2 = 1 - p(r) - \int_a^r \frac{1}{q}(\frac{r^2}{q})'dr. \tag{57}$$

An estimation of g_2 with $q = 2$, $a = 0.3$, $p = 0.05$, gives $|g_2| \simeq |-0.05 + 0.3^2/4| \simeq 0.03 \ll 1$, which is indeed very small.

We can also find that the Boozer coordinate (55) is the same as (50).

The Jacobian

$$\mathcal{J} = [\nabla\phi\cdot(\nabla\psi\times\nabla\theta_b)]^{-1} = [r\nabla\phi\cdot(\nabla r\times\nabla\theta_b)]^{-1} = \frac{R(1-\Delta'\cos\theta)}{1-(r+\Delta')\cos\theta} \simeq R^2 \simeq 1/B^2. \tag{58}$$

2.5 Forms in Hamada coordinate

We write the results directly here without detailed derivatives [need check],

$$\theta_h = \theta + (r-\Delta')\sin\theta, \qquad \zeta_h = \phi + 2qr\sin\theta, \tag{59}$$

with Jacobian

$$\mathcal{J} = [\nabla\zeta_h\cdot(\nabla\psi\times\nabla\theta_h)]^{-1} \simeq 1. \tag{60}$$

2.6 Zero shift

A zero shift or concentric circular geometry is simple and useful which is widely used for test problems. The well-known s-α Cyclone benchmark[10] is in fact $\alpha = 0$, i.e., concentric circular.

To give all variables analytically, we need special form of q profile to avoid numerical integral of $r(\psi_p) = \sqrt{2\int q d\psi_p}$, where we have used $\psi_t = r^2/2$ and $d\psi_t/d\psi_p = q$. A usual choice is

$$q = q_1 + q_2\hat{r}^2, \tag{61}$$

[9] Note: the transformation $\frac{\partial\theta_b}{\partial\theta} = \frac{1}{R(1-\Delta'\cos\theta)}$, gives $\theta_b = \theta - (r-\Delta')\sin\theta$, which is incorrect. Thanks Dr. F. Zonca points out to me this.

[10] Dimits *et al.*, PoP, 7, 969 (2000).

where $\hat{r} = r/a$, or

$$q = q_1 + q_2\hat{\psi}_p + q_3\hat{\psi}_p{}^2, \tag{62}$$

where $\hat{\psi}_p = \psi_p/\psi_w$, with ψ_w the wall ψ_p.

For (61), we get

$$\psi_p = \frac{a^2}{2q_2}\ln\Big(1 + \frac{2q_2}{a^2q_1}\psi_t\Big) = \frac{a^2}{2q_2}\ln\Big(1 + \frac{q_2}{q_1}\hat{r}^2\Big). \tag{63}$$

For (62), we get

$$\psi_w\Big(q_1\hat{\psi}_p + \frac{q_2}{2}\hat{\psi}_p{}^2 + \frac{q_3}{3}\hat{\psi}_p{}^3\Big) = \frac{r^2}{2}, \tag{64}$$

gives

$$\psi_p = \frac{r^2}{2\bar{q}}, \tag{65}$$

with $\bar{q} = q_1 + q_2\hat{\psi}_p + q_3\hat{\psi}_p{}^2$ and $a = 2\bar{q}(1)\psi_w$.

Other variables can be found in previous sections, and some of them are: $R = 1 + rcos\theta$, $B = \sqrt{B_t^2 + B_p^2}$, $B_t = 1/R = 1 - r\cos\theta$, $B_p = r/qR$, $g = 1$, $I = r^2/q$, $\delta = 0$. Usually, we use flux (Boozer) coordinate, then one should note $\theta = \theta_0 - r\sin\theta_0$. So, to $O(\epsilon^2)$, we can use

$$R = 1 + r_f\cos\theta_f - r^2\sin^2\theta_f, \tag{66a}$$
$$Z = r_f\sin\theta_f + r_f^2\sin\theta_f\cos\theta_f, \tag{66b}$$
$$B = 1 - r_f\cos\theta_f + r_f^2. \tag{66c}$$

However, form as (66) is not a good choice when $\Delta(r) \neq 0$. This form (see also Ref.[8]) can be used for analytical study, but bad for numerical study because flux surface would not be circles any more.

3 Applications

Shift circular equilibrium is useful since it is a good approximation and can gives arbitrary p, q profile easily and also has explicit flux coordinate expressions. While in numerical equilibrium, usually q profile is calculated after solving the G-S equation[11]. And we need numerical mapping of the flux coordinate.

3.1 GTC

In fact, the main motivation to write this document is from adding shift circular equilibrium to GTC.

For GTC (or R. B. White's ORBIT), we need calculate/input parameters: $q(r)$, $p(r)$, $\psi(r)$[12], Δ, Δ', R, Z, B, I, g, δ, ν, $\mathcal{J}$.

[11] Some codes can choose q-profile, e.g., JSOLVER

[12] Note: Here, we mean ψ_p. Please be careful of both normalizations and notations in practical applications.

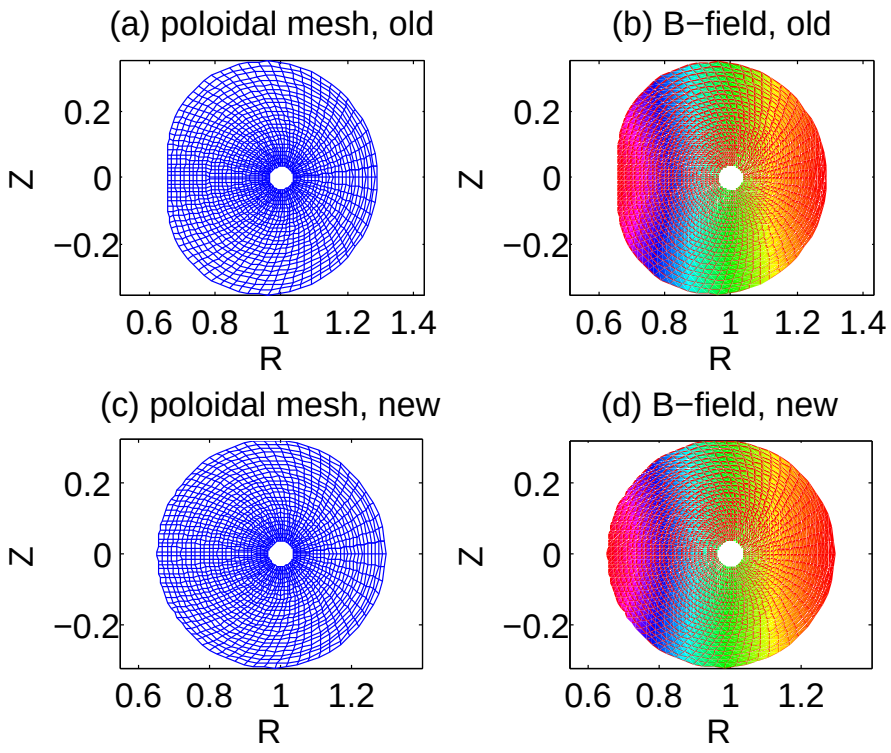

Figure 6: Grid mesh and B field for GTC, using old and new method, with Shafranov shift.

3.1.1 Profiles

We hope the $q(r)$, $p(r)$ or shear $s = \frac{rdq}{qdr}$ or gradient $d\ln(f)/dr$ profiles can be arbitrary. One can use analytical functions as in subsection 2.6 to model profiles. However, to choose good functions is not easy. Reading data from experiments or other codes (e.g., TRANSP) is also a choice.

Usually, we need numerical integral here now, especially for ψ_p and Δ.

Widely used profiles are $f \propto 1.0 + f_1\{\tanh[(f_2 - \hat{\psi})/f_3] - 1.0\}$ or $d\ln(f)/dr \propto \exp\{-[(r - r_1)/r_2]^6\}$[13].

Here, we use N-point (we use default N=11) fitting method, which is simple, general to model arbitrary profiles with enough accuracy.

We have two ways to add Shafarnov equilibrium to GTC: one is writing to GTC Fortran code directly as previous concentric circular analytical equilibrium; another is generating 'profile.dat' and 'spdata.dat' to be read by GTC numerical equilibrium part.

To keep original GTC code neat, we use the latter way. MATLAB code 'profile_generator.m' is to provide 'profile.dat' and be read by 'shafeq_spdata.m' to provide 'spdata.dat'.

Several choices are provided in 'profile_generator.m': one can use analytical profile, N-point fitting profile or read data from TRANSP outputs.

In 'shafeq_spdata.m', to get 'spdata.dat', we need interpolation and mapping. Two other func-

[13] E.g., Z. Lin and T. S. Hahm, PoP, 11, 1099-1108 (2004).

tions 'spln1d.m' and 'spln2d.m' are required, which will be discussed in the next subsection.

3.1.2 Mapping

The basic ideal is using B-spline. The 1D spline mapping in ψ is as

$$f(\psi) = f(1,i) + f(2,i)h + f(3,i)h^2, \tag{67}$$

where $\psi_i \le \psi \le \psi_{i+1}$, $h = \psi - \psi_i$, $i = 0, 1, ..., N$, and uniform grid size is assumed. Thus, $f'(\psi) = f(2,i) + 2hf(3,i)$. The coefficients $f(1:3,i)$ are calculated using 'spln1d.m'.

The 2D spline mapping in (ψ, θ) is

$$\begin{aligned} f(\psi,\theta) &= f(1,i,j) + f(2,i,j)\Delta\psi + f(3,i)\Delta\psi^2 + f(4,i,j)\Delta\theta + f(5,i)\Delta\psi\Delta\theta \\ &\quad + f(6,i,j)\Delta\theta\Delta\psi^2 + f(7,i)\Delta\theta^2 + f(8,i,j)\Delta\psi\Delta\theta^2 + f(9,i)\Delta\psi^2\Delta\theta^2, \end{aligned} \tag{68}$$

and the coefficients $f(1:9,i,j)$ are calculated using 'spln2d.m'. The derivatives of $f(\psi,\theta)$ are also easily to obtain.

Details discussion of the B-spline used in GTC can be found in Ref.[10].

Here, 'spln1d.m' and 'spln2d.m' I used are updated from ORBIT code.

3.1.3 Implement

In GTC previous zero-shift analytical equilibrium, R, Z and B are calculated using (66). As mentioned, this will caused deformation of flux surface. So, we use new treatment as proved in Sec.2.3. It seems the interpolation to calculated θ_f v.s. θ_s is not that necessary when $\eta \equiv r + \Delta'$ is small, say $\eta \le 0.5$, so we use (51) and $B = 1/R$.

However, for ballooning mode case, η is usually large. We choose interpolation for these cases.

The grid mesh and B field using old and new method with Shafranov shift are shown in Fig.6. From panels (a) and (b), we can see the deformation of flux surface when using old treatment when $\Delta \neq 0$. Anyway, 'shafeq_spdata.m' proves both options.

3.1.4 Benchmark

We use the Cyclone case to benchmark[14] the new equilibrium with GTC old analytical equilibrium (i.e., 'analytic.F90' and subroutine analyticeq in 'eqdata.F90').

The real frequency and growth rate is compared in Table1: (a) old, (b) new ($\Delta = 0$), (c) new ($\Delta \neq 0$). The error between (a) and (b) is aroud 3% though they should be the same, which may caused by the spline function, since (a) is calculated analytically, which (b) is calculated numerically from discrete grids. Comparing (c) with (a), we also find that the shift has merely a slight stabilized effect to ITG, i.e., to discuss ITG, ignoring Shafranov shift would not affect the results too much.

[14]Default electrostatic benchmark of FULL, GTC and GT3D can be found in [Rewoldt2007] G. Rewoldt, Z. Lin and Y. Idomura, Linear comparison of gyrokinetic codes with trapped electrons, Computer Physics Communications, 2007, 177, 775.

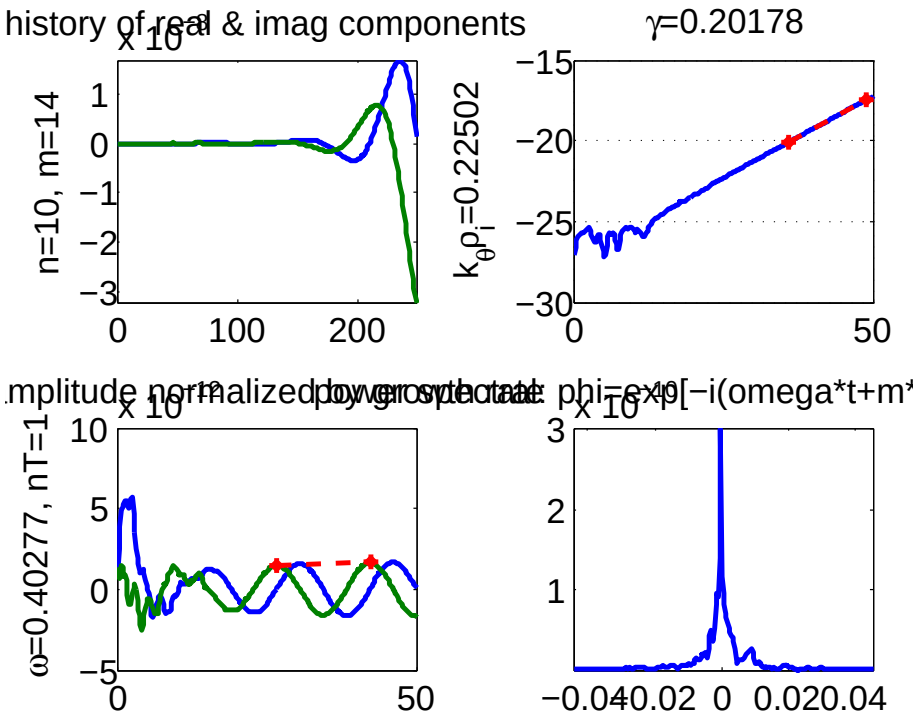

Figure 7: The time history data for new equilibrium (c) with $\Delta \neq 0$.

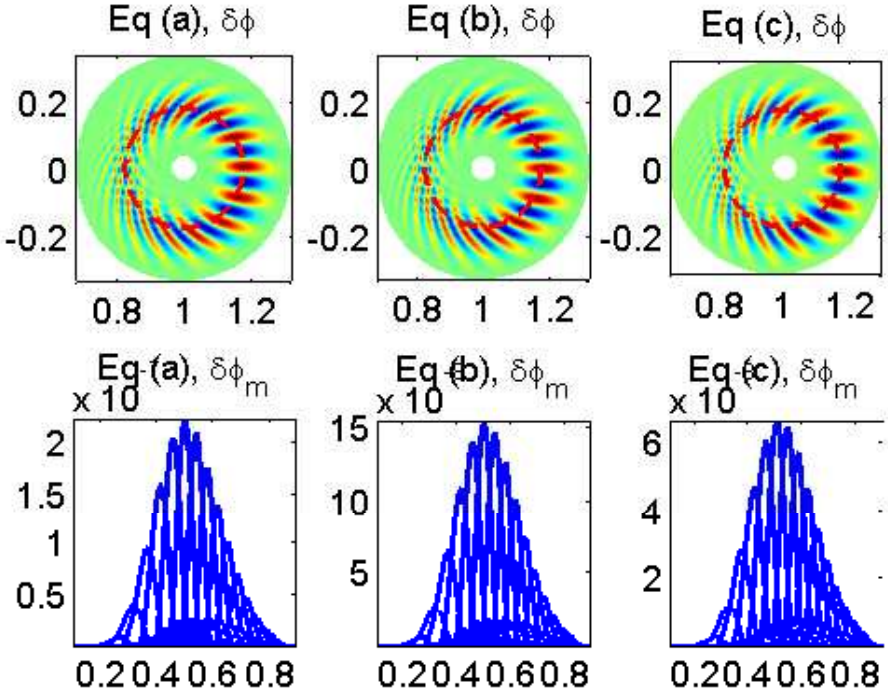

Figure 8: GTC snapshots of $\delta\phi$ for three equilibriums.

Table 1: GTC equilibrium benchmark

	(a) old	(b) new ($\Delta = 0$)	(c) new ($\Delta \neq 0$)
ω_r	0.408	0.403	0.403
γ	0.214	0.208	0.202

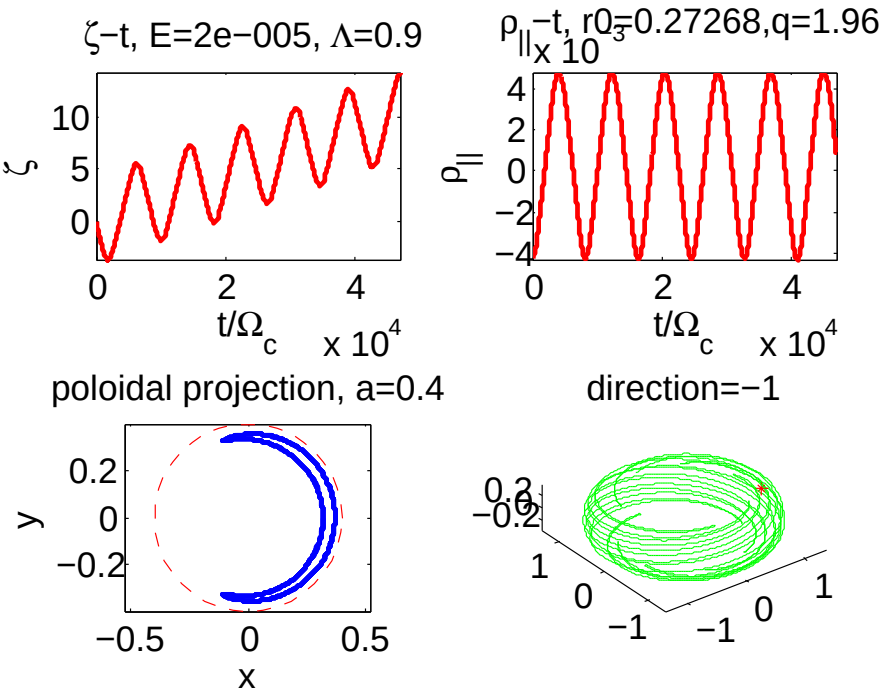

Figure 9: Guiding center orbit with concenteric circles equilibrium.

Fig.7 shows the time history data for new equilibrium (c). The poloidal cross section snapshots of $\delta\phi$ for three equilibriums are shown in Fig.8.

3.2 orbit.m

At present, we only use the concenteric circles equilibrium, with q-profile (62).

A typical run shown in Fig.9 is calculated using the subroutine 'OrbitGC_qpsip.m' in the 'orbit.m' code[15].

Details are provided in 'orbit.m' document. This code is public. You can modify it as yourself. However, please acknowledge it or cite the URL if it is useful.

[15]See `http://ifts.zju.edu.cn/forum/viewtopic.php?f=18&t=594`. This code calculates full orbit in general EM field such as dipole and tokamak, and also tokamak guiding center orbit using R. B. White's fomula[1].

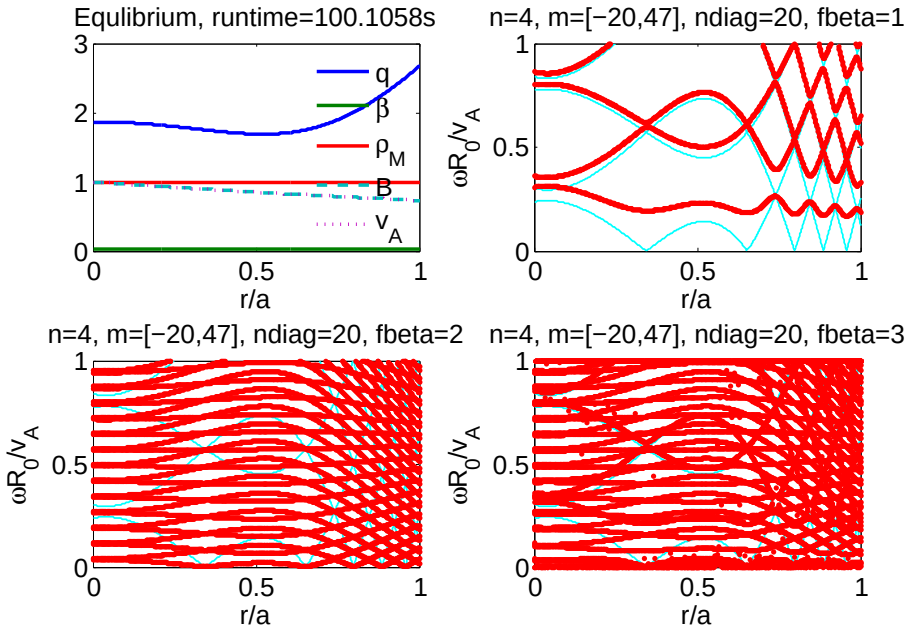

Figure 10: A typical Alfvén continuum calculated by 'awcon.m', with and without slow sound approximation.

3.3 awcon.m

At present, we only use the concenteric circles equilibrium, but the equilibrium parameters such as $q(r)$, $p(r)$ are arbitrary. The 'awcon.m'[16] code is developed to help quickly understand how to calculate Alfvén continuum, which is a simplified version of W. J. Deng's ALCON[11], i.e., 'awcon.m' only calculates the concenteric circles equilibrium case (then, the FFT part to transform numerical equilibrium is not needed) and thus very short.

A typical Alfvén continuum is shown in Fig.10. See 'awcon.m' document for details.

3.4 AMC

AMC[12] (Alfvén Mode Code[17]) calculated both Alfvén continuum and eigenmode using general shift circle equilibrium, which solves the vorticity equation (shear Alfvén law)

$$\begin{aligned}\nabla\cdot\big(\frac{\omega^2}{v_A^2}\nabla_\perp\delta\phi\big)+\mathbf{B}\cdot\nabla\big(\frac{1}{B^2}\nabla\cdot B^2\nabla_\perp Q\big)-\\ \nabla\big(\frac{J_\parallel}{B}\big)\cdot(\nabla Q\times\mathbf{B})+2\frac{\kappa\cdot(\mathbf{B}\times\nabla\delta P)}{B^2}=0,\end{aligned}\tag{69}$$

where, $\kappa=\mathbf{b}\cdot\nabla\mathbf{b}$, $Q=(\mathbf{b}\cdot\nabla\delta\phi)/B$, $\delta P=(\mathbf{b}\times\nabla\delta\phi\cdot\nabla P)/B$, $J_\parallel=\mathbf{b}\cdot\nabla\times\mathbf{B}$. Eq.(69) holds for large aspect ratio ($\epsilon=r/R\ll 1$) tokamak plasma to second order, and we have assumed low beta $\beta\sim O(\epsilon^2)$.

[16] See, `http://ifts.zju.edu.cn/forum/viewtopic.php?f=18&t=748`.
[17] Named by W. Chen.

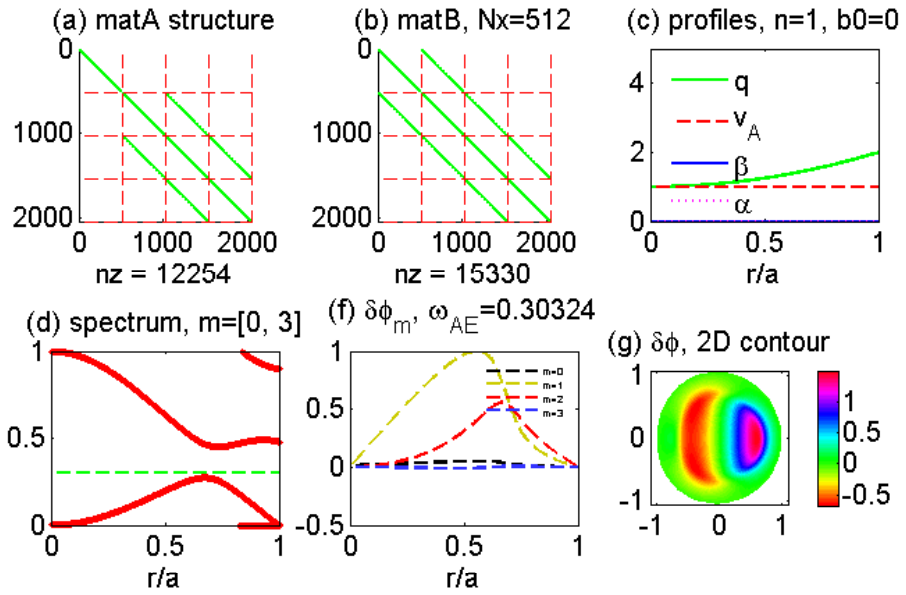

Figure 11: TAE in Fu1989, $\omega_{\rm TAE}^{\rm Fu89} = 0.31$, $\omega_{\rm TAE}^{\rm NOVA} = 0.3127$, $\omega_{\rm TAE}^{\rm KAEC} = 0.302$, $\omega_{\rm TAE}^{\rm AMC} = 0.303$.

Besides Alfvén eigenmodes (GAE, TAE, RSAE and more), AMC also supports unstable internal kink mode as well as ideal ballooning mode (IBM).

Fig.11 shown the TAE result with[18]: $q = 1.0 + 1.0(r/a)^2$, $\rho = 1.0$, n=1 and $R_0/a = 4$.

4 Ballooning Mode

The local $s - \alpha$ equilibrium is widely used for ballooning mode, since the ballooning representation.

4.1 Ballooning mode representation

4.2 Ideal ballooning mode

For s-α model to calculate the ballooning mode, the usual definition is $\alpha \equiv -q^2 R \frac{d\beta}{dr} \simeq \Delta'$. To access the second stability domain, we usually need $\alpha > 1$ or $\gg 1$. While, from (42), $\Delta' > 1$ is forbidden.

The problem is from the approximation $\alpha \simeq \Delta'$. A more reasonable mode equation for ideal ballooning mode should be (see also p131 in Ref.[1])

$$\frac{\partial}{\partial\theta}[1 + h^2(\theta)] \tag{70}$$

[not correct, $\alpha \simeq r\Delta''$]

[18] G. Y. Fu and J. W. V. Dam, PFB, 1, 1949.

4.3 Test in GTC

It seems we should keep $r \leq 0.4$, $r + \Delta' \leq 0.5$. Otherwise, the θ around the wall flux surface would not be handled correctly.

Communications and discussions with Fulvio Zonca, Yong Xiao, You-Wen Sun, Joseph McClenaghan, You-Jun Hu, Zhi-Xin Lu, Tai-ge Zhang, Christopher Wrench, Wen-jun Deng and Andreas Bierwage improved this document a lot.

References

[1] R. B. White, *The Theory of Toroidally Confined Plasmas*, World Scientific Imperial College Press, 2001.

[2] R. D. Hazeltine and J. D. Meiss, *Plasma Confinement*, Perseus Books, 1992.

[3] S. Jardin, *Computational Methods in Plasma Physics*, CRC Press, 2010.

[4] W. D. DHaeseleer, W. N. G. Hitchon, J. D. Callen and J. L. Shohet, *Flux Coordinates and Magnetic Field Structure: A Guide to a Fundamental Tool of Plasma Theory*, Springer, 1991, 228.

[5] V. D. Shafranov, *Reviews of Plasma Physics, Vol. 2*, p. 103, Consultants Bureau, New York, 1966.

[6] F. Zonca, IFTS Intensive Course on Advanced Plasma Physics, Spring 2009, `http://www.afs.enea.it/zonca/references/seminars/IFTS_spring09/`.

[7] L. L. Lao, R. M. Wieland, W. A. Houlberg and S. P. Hirshman, VMOMS – A computer code for finding moment solutions to the Grad-Shafranov equation, Computer Physics Communications, 1982, 27, 129 - 146.

[8] J. D. Meiss and R. D. Hazeltine, Canonical coordinates for guiding center particles, Physics of Fluids B: Plasma Physics, 1990, 2, 2563.

[9] H. J. de Blank and T. J. Schep, Theory of the m=1 kink mode in toroidal plasma, Physics of Fluids B: Plasma Physics, 1991, 3, 1136.

[10] Y. Xiao, I. Holod, Z. X. Wang, J. McClenaghan, Z. Lin and T. G. Zhang, Mircoturbulence simulation in general geometry, to submit.

[11] W. Deng, Z. Lin, I. Holod, Z. Wang, Y. Xiao and H. Zhang, Linear properties of reversed shear Alfvén eigenmodes in the DIII-D tokamak, Nuclear Fusion, 2012, 52, 043006.

[12] H. S. Xie and Y. Xiao, Parallel equilibrium current effects on the existence of reversed shear Alfvén eigenmodes, to submit.